Environmental Science and Pollution Research (2023) 30:85210–85222
https://doi.org/10.1007/s11356-023-28308-z

RESEARCH ARTICLE

Synthesis of submicron ferrous oxalate from red mud with high Fenton catalytic performance on degradation of methylene blue

Yuxin Yang[1,2] · Ning Wang[1] · Hannian Gu[1,2]

Received: 4 February 2023 / Accepted: 13 June 2023 / Published online: 29 June 2023

Abstract

Ferrous oxalate dihydrate (FOD) can be used as a photo-Fenton catalyst with remarkable photo-Fenton catalytic and photocatalytic performances on organic pollutant degradation. Various reduction processes were compared in the current study to synthesize FODs from ferric oxalate solution utilizing the iron source in alumina waste red mud (RM), including natural light exposure (NL-FOD), UV light irradiation (UV-FOD), and hydroxylamine hydrochloride hydrothermal method (HA-FOD). The FODs were characterized and employed as photo-Fenton catalysts for methylene blue (MB) degradation, and the effects of HA-FOD dosage, H_2O_2 dosage, MB concentration, and the initial pH were investigated. The results show that HA-FOD has submicron sizes and lower impurity contents with more rapid degradation rates and higher degradation efficiencies compared with the other two FOD products. When using 0.1 g/L of each obtained FOD, 50 mg/L of MB can be rapidly degraded by HA-FOD by 97.64% within 10 min with 20 mg/L of H_2O_2 at pH of 5.0, while NL-FOD and UV-FOD achieve 95.52% in 30 min and 96.72% in 15 min at the same conditions, respectively. Meanwhile, HA-FOD exhibits strong cyclic stability after two recycling experiments. Scavenger experiments reveal that the predominant reactive oxygen species responsible for MB degradation are hydroxyl radicals. These findings demonstrate that submicron FOD catalyst can be synthesized using hydroxylamine hydrochloride hydrothermal process from ferric oxalate solution with high photo-Fenton degradation efficiency and reduced reaction time for wastewater treatment. The study also provides a new pathway of efficient utilization for RM.

Keywords Advanced oxidation processes · Heterogeneous Fenton · Dye degradation · Solid waste · Hydrothermal reduction · Kinetic model

Responsible Editor: Ricardo A. Torres-Palma

Highlights

1. Iron source in waste red mud was reused to synthesize different FOD products.
2. Through HA reduction from ferrioxalate solution to obtain HA-FOD.
3. HA-FOD was synthesized with submicron size and less impurities.
4. HA-FOD presents high efficiency in photocatalysis and photo-Fenton process.

✉ Hannian Gu
guhannian@vip.gyig.ac.cn

[1] Key Laboratory of High-Temperature and High-Pressure Study of the Earth's Interior, Institute of Geochemistry, Chinese Academy of Sciences, Guiyang 550081, China

[2] University of Chinese Academy of Sciences, Beijing 100049, China

Abbreviations

AOPs	Advanced oxidation processes
ROSs	Reactive oxygen species
FOD	Ferrous oxalate dihydrate
RM	Red mud
NL-FOD	Ferrous oxalate dihydrate obtained under natural light irradiation
UV-FOD	Ferrous oxalate dihydrate obtained under UV irradiation
MB	Methylene blue
HA	Hydroxylamine hydrochloride
HA-FOD	Ferrous oxalate dihydrate obtained by HA hydrothermal reduction

Introduction

Advanced oxidation processes (AOPs) are chemical oxidation methods for contaminant degradation by reactive oxygen species (ROSs) (Miklos et al. 2018; Lin et al. 2022). As one of the most cost-effective AOPs, Fenton process has attracted great attentions in recent years for removing recalcitrant compounds with •OH (hydroxyl radical) from sewage and accomplishing high mineralization levels (Oturan and Aaron 2014; Pliego et al. 2015; Mohadesi et al. 2021). However, the reduction of Fe^{3+} to Fe^{2+} remains the speed limit step for producing ROSs in a heterogeneous Fenton system, constraining the efficiency of the catalyst to oxidize the pollutants (Lai et al. 2021). The efficiency of Fenton reaction can be increased by combining with assistant approaches like UV or sonic irradiation, in which process more •OH is generated and the regeneration of the Fe^{2+} catalyst from Fe^{3+} is facilitated (Karimi et al. 2020; Ribeiro and Nunes 2021; Brillas 2022). Meanwhile, organic complexing agents are commonly introduced to traditional Fenton system to accelerate the catalytic process (Wang et al. 2016, 2019c). For example, a multitude of organic pollutants can be rapidly degraded by adding oxalic acid as complexing agents to form photosensitive complexes ferrioxalate with Fe^{3+}, speeding up the generation of hydroxyl radical due to its oxalate ligand and lower pH (Dias et al. 2014; Baba et al. 2015; Vorontsov 2019; Zhang and Zhou 2019).

Ferrous oxalate dihydrate (FOD) is the simplest coordination polymer photocatalyst consisting of Fe^{2+} and oxalate ligand, which possesses the advantages of oxalate complex in Fenton reaction and shows remarkable photocatalytic and photo-initiated Fenton capacity in the degradation of organic pollutants (Fan et al. 2016; Bi and Dong 2021). As an efficient heterogeneous photo-Fenton catalyst, FOD can activate hydrogen peroxide (H_2O_2) or persulfate and generate ROSs due to its high photosensitivity and self-activation capacity as $C_2O_4^{2-}$ in the catalyst can reduce Fenton-generated Fe^{3+} to Fe^{2+}, thus increasing the reaction rate (Li et al. 2018; Hu et al. 2019; Chen et al. 2022; Wu et al. 2022). In addition, FOD is also used as absorbents for the removal of dyes and heavy metals from the contaminated systems (Dhal et al. 2015; Zeng et al. 2021; Huang et al. 2022). Traditionally, Fenton catalyst FOD is mainly prepared by mixing ferrous salts with oxalic acid or oxalates (Hu et al. 2019; Wang et al. 2019a). Exceptionally, Liu et al. (2016) synthesized FOD by direct ball milling of iron with oxalic acid. The preparation of FOD as photo-Fenton catalyst through the reduction of soluble ferrioxalate complex has not been reported. It is of great significance to investigate alternative techniques of preparing ferrous oxalate ferrioxalate complex through reduction process for further research and economic value.

Such a direct reduction process needs the soluble ferrioxalate complex solution as reactant that can be obtained using oxalic acid to extract iron from iron-rich industrial solid waste. Red mud (RM) is an alkaline waste by-product discharged during the alumina manufacturing process (Agrawal and Dhawan 2021; Li et al. 2022c). The enormous storage and annual discharge of RM have exceeded 4.6 billion tons and 200 million tons worldwide, respectively (Xue et al. 2019; Li et al. 2022c), which might cause long-term environmental impacts. RM stockpiling occupies considerable land areas and tends to produce dust contaminating the air. The leachate with high alkalinity will pollute groundwater and cause soil salinization, posing a serious threat to the nearby ecosystem (Khairul et al. 2019). Therefore, RM reduction, resourceful utilization, and harmless treatment have become the essential requirement for sustainable development. RM contains high iron oxide concentration and can be recycled and utilized as a potential iron resource (Bento et al. 2016; Liu et al. 2021). It is proposed that oxalic acid leaching is a promising process with a strong ability for selectively extracting iron from RM to dissolve hematite as soluble ferrioxalate complex solution (Agrawal and Dhawan 2021; Samal 2021; Li et al. 2022a). The dissolved ferrioxalate complex could catalytically be reduced to FOD under UV (UV-FOD) or the natural light irradiation (NL-FOD) (Yu et al. 2012; Gu et al. 2017; Tanvar and Mishra 2021). In this economical pathway, FOD is precipitated and can be applied as photo-Fenton catalyst to the degradation of contaminants (Hu et al. 2019) and precursor to produce iron oxide nanoparticle products (Angermann and Töpfer 2008; Liu et al. 2020). However, in addition to the reduction by UV or the natural light irradiation, other reduction of Fe^{3+} from ferrioxalate complex solution to prepare FOD has not been reported. In the meantime, using the obtained FOD products as iron-based Fenton catalysts for the treatment of sewage might be a new value-added application.

Methylene blue (MB) is an organic thiazine dye with strong biological toxicity and poor biodegradability, posing a threat to environment and human health (Rahimi et al. 2014; Tkaczyk et al. 2020; Sukhatskiy et al. 2022). MB is difficult to be degraded from contaminated water through traditional treatments, such as adsorption, coagulation, and biochemical processes. AOPs, specifically, photo-Fenton process is widely applied for the removal of MB, which could rapidly produce ROSs and mineralize refractory compounds in wastewater (Samsami et al. 2020). Therefore, employing FOD recycled from solid wastes as Fenton catalyst to degrade MB is a promising pathway to accomplish resource recovery and environmental remediation.

The current work aims to provide a novel method via a reductive hydrothermal process in the presence of hydroxylamine hydrochloride (HA) to synthesize FOD (HA-FOD) with enhanced Fenton catalytic performance on MB degradation from RM leachate of ferrioxalate complex solution. The catalytic performances of HA-FOD, NL-FOD, and UV-FOD catalysts were compared. The effects of initial conditions on the HA-FOD catalytic reaction were systematically studied. The reusability of the catalyst and the dominant ROSs contributed to MB degradation were also investigated to further understand Fenton catalytic degradation mechanism of HA-FOD.

Materials and methods

Materials and reagents

The RM sample used in this research was collected from an alumina refinery in Qingzhen, Guizhou Province of China. The main chemical components of RM sample were widely reported as Al_2O_3, Fe_2O_3, CaO, Na_2O, K_2O, and SiO_2 (Li et al. 2022b; Hajjaji et al. 2016). The fresh RM contained 30% of water, and it was dried to a constant weight. Then it was crushed and screened to less than 75 μm for further use. Oxalic acid (≥ 99.5 wt%) was applied to dissolve iron in the leaching process. HA (≥ 98.5 wt%) was used as a reductant to synthesize FOD, and H_2O_2 (≥ 30 wt%) was used to trigger the Fenton reaction. The reagents used in this study were all of analytical grade, and all the solutions were prepared with deionized water.

Preparation and characterizations of FOD catalysts

The scheme of catalyst preparation process is shown in Fig. S1. The prepared RM was leached using 1 mol/L oxalic acid with a liquid–solid ratio of 15:1 mL/g under 80 °C for 2 h, and Fe was enriched in the leaching solution according to previous report (Yu et al. 2012). Subsequently, Fe^{3+} in the solution was reduced in three pathways, and different FOD catalysts were obtained. The filtrate was fully exposed to natural light until the precipitate did not further increase, and afterwards NL-FOD was collected. UV-FOD was precipitated as the leachate was irradiated under a 250-W UV light (365 nm, GY-250, China) for 6 h. HA-FOD was synthesized via a hydrothermal treatment, in which process 0.35 g of HA was dissolved in 45 mL leached solution (HA: Fe = 1:1), and then the solution was transferred into a 100-mL Teflon-lined stainless-steel autoclave and heated at 130 ℃ for 7 h. After reaction, all the prepared FOD samples were separated by filtration, washed with deionized water and ethanol for several times, and dried at 60 ℃ overnight.

The morphology features of FOD catalysts were viewed by scanning electron microscopy (SEM, FEI Scios, USA) equipped with an energy-dispersive X-ray spectrometer (EDS). The particle size distribution was determined by laser particle size analyzer (Mastersizer 2000, UK). The chemical components of the catalysts were analyzed by X-ray fluorescence spectroscopy (XRF, PANalytical PW2424, Netherlands). The phase chemical compositions of catalysts were identified by X-ray diffractometer (XRD, PANalytical Empyrean, Netherlands) with a Cu Kα radioactive source scanning at the 2θ range from 4 to 70°. Fourier transform infrared spectrometer (FTIR, VERTEX 70, Germany) was employed to characterize variations of surface functional groups of different FOD samples. The surface element and valence of the catalysts were measured by X-ray photoelectron spectrometer (XPS, Thermo Scientific K-Alpha, USA) with C1s peak calibrating the binding energy at 284.8 eV.

Photo-Fenton degradation experiments of MB

In a typical process, 0.02 g of FOD catalyst (0.1 g/L) was dispersed in 200 mL MB solution (50 mg/L, pH = 5.0) in a thermostatic water bath (THZ-82A, China) with an agitation of 200 rpm at 25 ℃. The solution was stirred for 30 min in the dark to establish adsorption equilibrium. Then the photo-Fenton degradation experiment was initiated by adding 20 mg/L of H_2O_2 into the suspensions, which process was under a 250-W UV irradiation (365 nm, GY-250, China). At a time interval of the process, 2 mL of the solution was sampled at predetermined time intervals, filtered through a 0.45-μm filter film and quenched by 0.1 mL of n-butanol for further analysis. The concentration of MB was determined by UV–vis spectrophotometry (UV9100C, USA) at the wavelength of 664 nm. The concentrations of dissolved Fe after catalytic process were determined by inductively coupled plasma optical emission spectrometry (ICP-OES, Agilent 5110, USA). The effects of various experimental parameters on MB degradation efficiency were systematically explored, including FOD dosage (0.025–0.125 mg/L), H_2O_2 concentration (5–25 mg/L), initial MB concentration (40–80 mg/L), and initial pH (3, 5, 7, 9, and 11). The initial pH values of MB solutions were adjusted by NaOH and HCl solutions, and the pH values of the solutions were measured by a pH meter (pHS-SC, China). All degradation experiments were conducted in triplicate to effectively reduce the experimental error.

Kinetic constants of photo-Fenton experiments

MB degradation of FOD Fenton process was fitted by the pseudo-first-order kinetic model as previous studies in regard to FOD Fenton reaction (Chen et al. 2022; Wu et al. 2022). The model can be described as Eq. (1) (Zeng et al. 2020):

$$\ln\left(C/C_0\right) = -kt \quad (1)$$

where C_0 and C (mg/L) are the MB concentrations during the reaction at 0 min and a certain time t (min), respectively, and k (min^{-1}) represents the rate constant of pseudo-first order. The sampling time was set at 0, 3, 5, 7, 10, 12, 15, 20, and 30 min in the photo-Fenton experiments.

Results and discussion

Characterization of FOD catalysts

SEM images (Fig. 1a–c) demonstrate the surface morphology and particle size of the synthesized HA-FOD, NL-FOD, and UV-FOD products. The comparison of

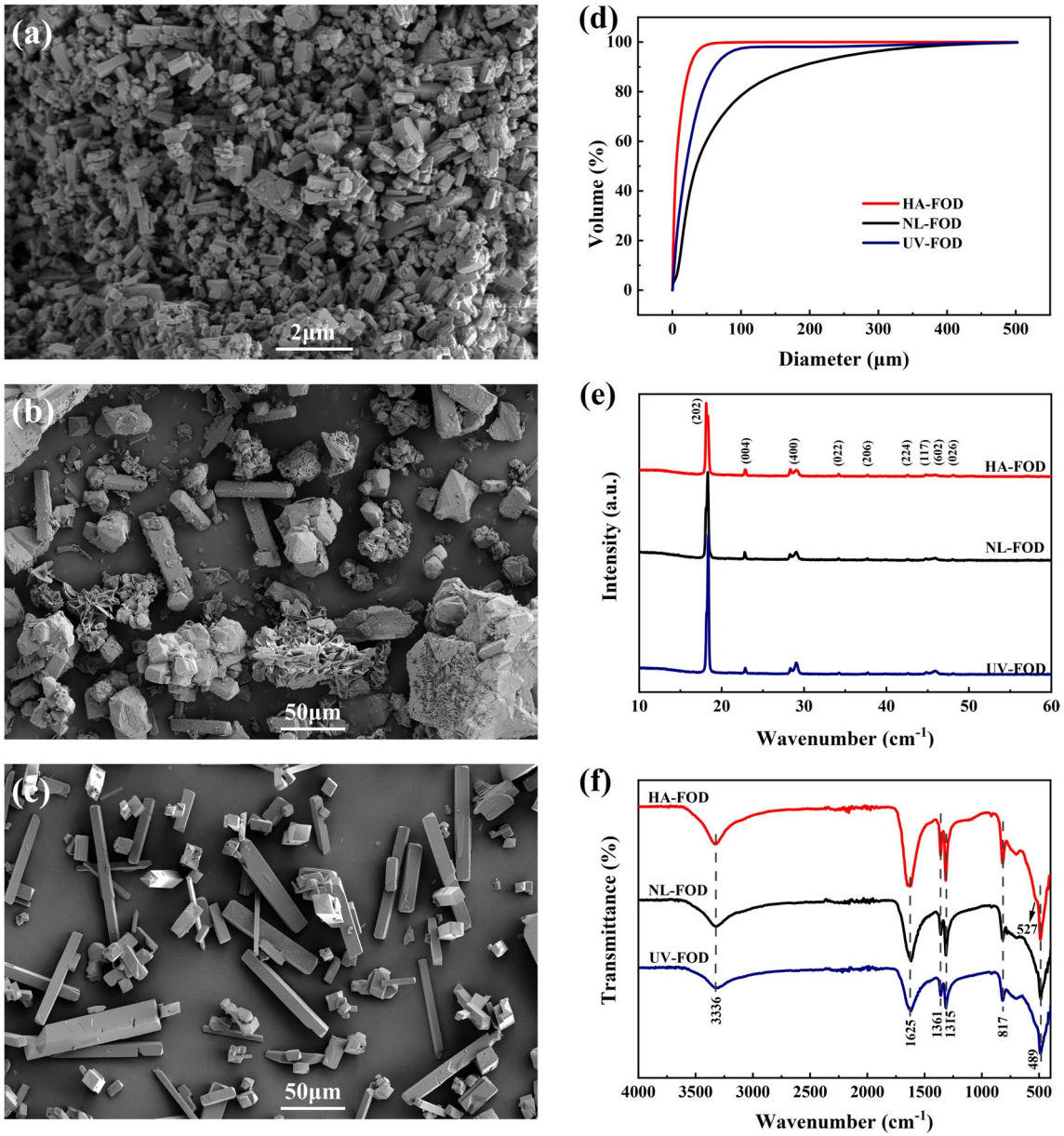

Fig. 1 **a** HA-FOD SEM image, **b** NL-FOD SEM image, **c** UV-FOD SEM image, **d** particle size distribution, **e** XRD patterns, and **f** FTIR spectra of the prepared catalysts

particle size distribution of the prepared FOD samples is depicted in Fig. 1d. These results implied that the particle size distribution of HA-FOD was more uniform than those of NL-FOD and UV-FOD. It can be observed that 50% of HA-FOD, NL-FOD, and UV-FOD particles were less than 6.303, 39.022, and 22.278 μm, respectively. The particle size distribution of HA-FOD particles was tinier than those of NL-FOD and UV-FOD.

Different from the results of particle size distribution, the microstructure of the prepared HA-FOD was composed of regular cuboid-like microrods from 100 nm to 1 μm in diameter, which was smaller than FOD products synthesized by directly mixing ferrous sulfate heptahydrate with potassium oxalate monohydrate or oxalic acid dihydrate in the previous studies with the cuboid particle sizes of 5–10 μm (Hu et al. 2019; Kim et al. 2020). This is because the size and structure of the synthesized materials can be precisely controlled by the hydrothermal reaction (Wang and Tang 2021). Meanwhile, fewer impurities can be observed by EDS spectrum (Fig. S2a). NL-FOD was comprised of complex structures with around 50 μm in the size. The results shown in Figs. 1b and S2b indicated that the particles of flakes clusters and irregular block-shape were indicative of calcium oxalate, and the rough rod-shape particles were FOD. UV-FOD possessed regular rod shape with the lengths of 10–100 μm and widths of 5–10 μm. It was identified as FOD particles, and the tiny clastic particles attached on its surface were calcium oxalate (Fig. S2c).

The crystallographic structure and phase chemical compositions of the samples were confirmed using XRD analysis as shown in Fig. 1e. The results confirmed that all the FODs obtained through various reduction reactions were the formation of β-FeC_2O_4•$2H_2O$, which was corresponded with the previous study (Kim and Baek 2019). There were nine prominent diffraction peaks for the prepared composite at 18.09, 22.84, 29.13, 34.18, 37.33, 42.59, 44.79, 45.79, and 48.03°, which correspond to (202), (004), (400), (022), (206), (224), (117), (602), and (026) planes of β-FeC_2O_4•$2H_2O$. Particularly, the diffraction peak of HA-FOD at 29.16° was broader compared to NL-FOD and UV-FOD, which was attributed to its smaller crystallite size according to the Scherrer's equation (Wang et al. 2020), and it is corresponding with the results analyzed from SEM results. There was no characteristic diffraction peak of other phase found in the XRD pattern probably because the impurities were of low contents.

The FTIR spectra of the prepared HA-FOD, NL-FOD, and UV-FOD are shown in Fig. 1f, which are all corresponded with FTIR patterns of β-FeC_2O_4•$2H_2O$. The stretching vibration of -OH was at 3336 cm^{-1} in the infrared spectrum (Liu et al. 2016; Zeng et al. 2021). The existence of $C_2O_4^{2-}$ was proved by the primary peaks at 1625, 1361, 1315, 817, and 489 cm^{-1}, responsible for C = O and C-O asymmetric stretching, C-O symmetric stretching peak, and C–C-O and O-C = O bending vibrations, respectively (Zeng et al. 2021). The characteristic absorption peak of Fe–O vibration band was at 527 cm^{-1} (Huang et al. 2022).

The main chemical components of the FOD samples were determined, and the results are presented in Table 1. In comparison with NL-FOD and UV-FOD catalysts, HA-FOD contained higher iron content and less impurity elements like Ca and Mg, which existed in the form of oxalates with inferior catalytic ability. The impurity of Ti was slightly higher, and it might enhance the photocatalytic capacity of HA-FOD (Mohamed and Besisa 2022). The main chemical

Table 1 Chemical compositions of the three prepared FOD catalysts (wt %)

Sample	Al_2O_3	CaO	Fe_2O_3	MgO	Na_2O	SiO_2	TiO_2	LOI
NL-FOD	0.62	2.30	37.99	0.53	0.30	0.12	0.11	57.40
UV-FOD	0.56	0.53	40.26	0.49	0.26	0.05	0.09	56.90
HA-FOD	0.78	0.09	40.32	0.22	0.36	0.15	0.29	56.99

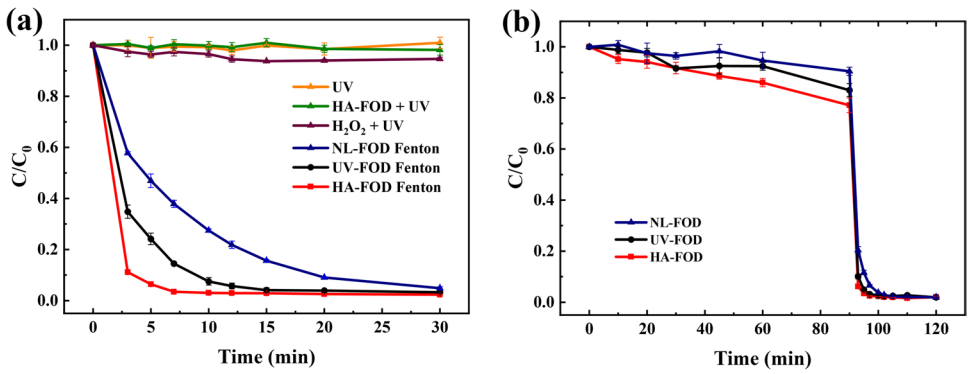

Fig. 2 **a** Comparison of MB degradation in different systems at optimal experimental conditions and **b** the comparison of joint photocatalytic and photo-Fenton process of the three catalysts. The experimental parameters apart from the investigated parameter fixed on pH 5.0, H_2O_2 20 mg/L, HA-FOD 0.10 g/L, MB 50 mg/L, and temperature 25 ℃

reaction for HA-FOD precipitation process can be summarized by Eq. (2) (Peng et al. 2016). In the reduction process, H^+ was generated, and the pH of the system was reduced, and this is the probable reason why more Ca and Mg dissolved in the solution and less impurities of Ca and Mg in the product of HA-FOD.

$$2Fe^{3+} + 2NH_2OH \bullet HCl \rightarrow 2Fe^{2+} + N_2 \uparrow + 4H^+ + 2H_2O + 2Cl^- \quad (2)$$

MB degradation with different FOD catalysts

The degradation of MB was evaluated under different experimental systems, and the catalytic performance of the synthesized different FOD catalysts was compared as shown in Fig. 2a. MB could rarely be removed under UV irradiation or HA-FOD + UV system at negligible degradation efficiencies of 0.09% and 1.83%, respectively. Notably, MB was continuously degraded in the presence of HA-FOD under UV irradiation, in accordance with the previous studies that FOD was also functional as a photocatalyst without H_2O_2 addition (Fan et al. 2016; Li et al. 2018). In comparison, the MB degradation efficiency of H_2O_2 + UV system was marginally higher at 5.42% after 30-min reaction, which could be ascribed to the weak oxidation capacity of H_2O_2 on MB (Zhu et al. 2020). In the FOD photo-Fenton systems, efficient MB degradation processes were accomplished at the rates of 97.64% for HA-FOD, 96.72% for UV-FOD, and 95.52% for NL-FOD, under the conditions of 0.1 g/L catalyst, 50 mg/L of MB, 20 mg/L of H_2O_2, and initial pH 5.0 at 25 ℃. These results suggested the high catalytic performances of all FOD catalysts on H_2O_2 activation. The final MB degradation efficiency of HA-FOD was slightly higher than those of UV-FOD and NL-FOD. Moreover, HA-FOD completed the MB degradation within 10 min, much shorter than those of UV-FOD (15 min) and NL-FOD (30 min) as shown in Fig. 2a. The degradation curves of MB in FOD photo-Fenton processes were fitted by the pseudo-first-order kinetic model (Fig. S3). The kinetic rate constants of HA-FOD, UV-FOD, and NL-FOD were calculated as 0.4747, 0.2217, and 0.1008 min^{-1}, and the relevant R^2 were 0.9395, 0.9722, and 0.9687, respectively. The superior removal efficiency of HA-FOD could be attributed to lower the impurity contents and especially its smaller particle diameter as discussed, which provided more active sites and accelerated the reaction.

Due to the high-efficient photocatalytic performance, FOD could initiate a combined photocatalytic and photo-Fenton reactions without the addition of H_2O_2 (Fan et al. 2016). Therefore, we proposed a joint photocatalysis and photo-Fenton process in which the MB solution was pretreated by photocatalytic reaction with FOD but without H_2O_2 introduction under the UV irradiation, and then the photo-Fenton process was initiated by adding H_2O_2. The photocatalytic ability of the three prepared catalysts is compared in Fig. 2b. It can be seen that after 90-min UV irradiation, HA-FOD showed the greatest photocatalytic ability on MB degradation by the rate of 22.87%, while UV-FOD and NL-FOD were at 16.94% and 9.52%, respectively. Subsequently, the reaction was greatly accelerated as H_2O_2 was added to the system at 90 min to provide abundant radicals of •OH. This joint photocatalysis and photo-Fenton process were capable to save more than 20% of the H_2O_2, thus reducing the cost of reagent in practical sewage treatment application.

Effects of reaction parameters on MB degradation in HA-FOD Fenton process

Since HA-FOD exhibited the strongest photo-Fenton catalytic performance in comparison with the other two FOD catalysts, a series of comparative experiments were carried out to obtain the optimal experimental parameters of HA-FOD on the degradation of MB. The effect of HA-FOD dosage on MB degradation was first investigated at the conditions of initial MB concentration of 50 mg/L, H_2O_2 dosage of 20 mg/L, and initial pH of 5.0. The HA-FOD dosage of 0.025, 0.050, 0.075, 0.100, and 0.125 g/L were employed, and the results are presented in Fig. 3a. With the addition of HA-FOD increasing from 0.025 to 0.100 g/L, the reaction time of achieving the degradation equilibrium effectively shortened, and the kinetic rates largely enhanced from 0.1172 to 0.4743 min^{-1} (Fig. 3b). This phenomenon could be ascribed to that the increasing quantity of catalysts provided more active sites, which promoted the processes of H_2O_2 decomposition and therefore yielded more •OH. However, when the concentration of HA-FOD increased from 0.100 to 0.125 g/L, the rate constant of degradation on MB enhanced slightly to 0.5100 min^{-1}. This could be assigned to the fact that excessive ferrous ions could also capture •OH (Niveditha and Gandhimathi 2020), resulting in an unobvious change of degradation on MB. Consequently, a comparatively minimal catalyst dosage at 0.100 g/L was chosen as the optimum dosage.

The oxidation of MB with various H_2O_2 concentrations is illustrated in Fig. 3c. When H_2O_2 concentration raised from 5 to 20 mg/L, the degradation rate increased from 46.49 to 97.64%, with the kinetic constant dramatically increasing from 0.0263 to 0.4747 min^{-1} (Fig. 3d), which proved the critical role of H_2O_2 in photo-Fenton process. This could be explained by the fact that the increasing concentration of H_2O_2 could generate more hydroxyl radicals with strong oxidation ability on MB degradation. Nevertheless, further addition of 25 mg/L H_2O_2 could hardly enhance the degradation efficiency at 97.69% but hindered the degradation with k falling from 0.4747 (20 mg/L) to 0.3567 min^{-1} (25 mg/L). The scavenging effect of •OH by H_2O_2 might be responsible

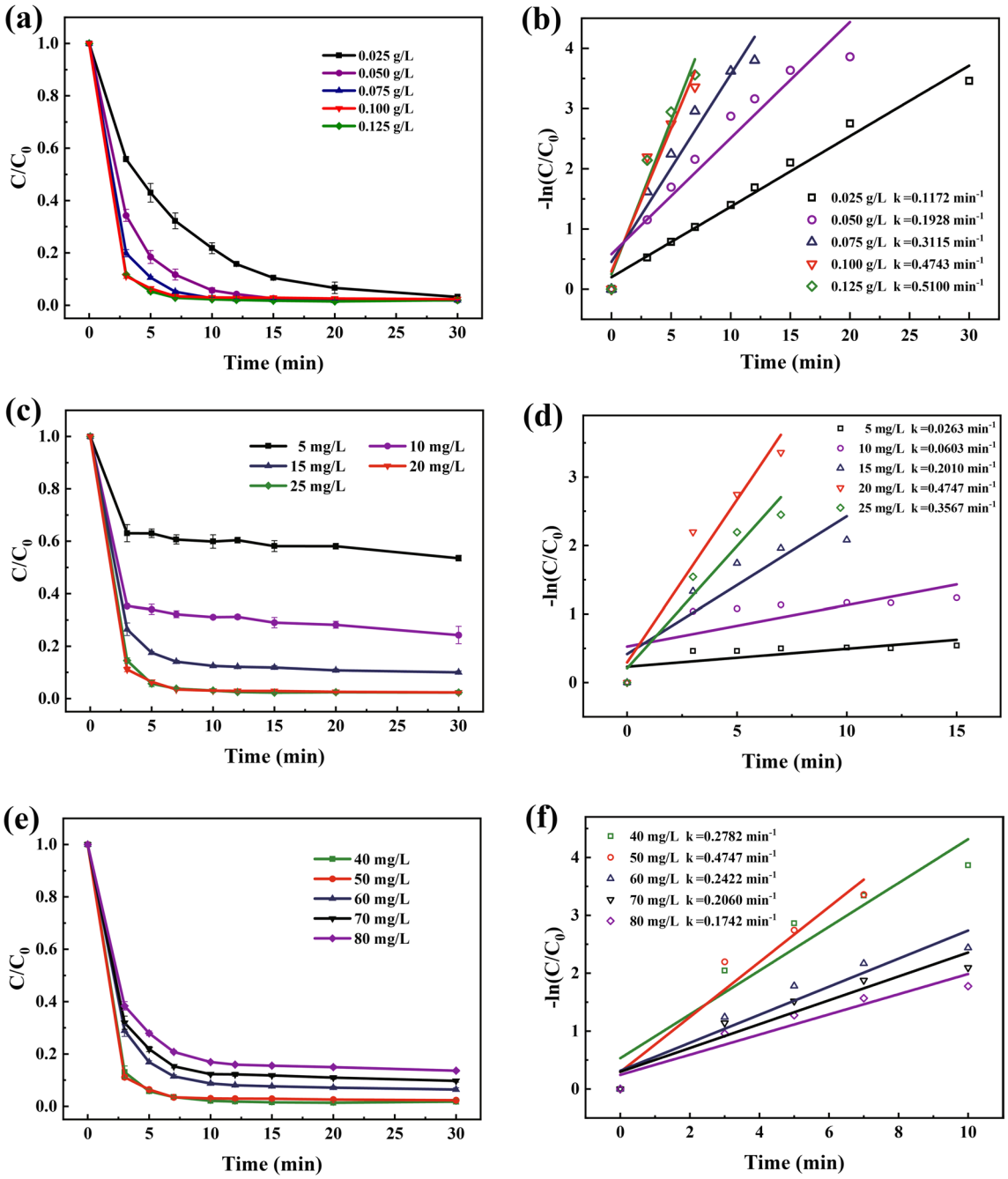

Fig. 3 Effect of the experimental parameters on MB degradation and the corresponding kinetic curves: **a**, **b** HA-FOD dosage; **c**, **d** H_2O_2 concentration; **e**, **f** initial MB concentration; **g**, **h** initial solution pH; and **i** pH and the concentration of Fe ions of the solution after reaction under different initial pH values. The experimental parameters apart from the investigated parameter fixed on pH 5.0, H_2O_2 20 mg/L, HA-FOD 0.10 g/L, MB 50 mg/L, and temperature 25 ℃

for the phenomenon. Despite additional oxidants such as HOO• and O_2• are produced, their oxidation potentials were significantly lower than •OH and contributed far less to the degradation of MB (Ferroudj et al. 2017).

Initial MB concentration was another significant factor affecting the degradation process, and the results are shown in Fig. 3e. With the decrease of initial MB concentration from 50 to 40 mg/L, the kinetic rate reduced from 0.4747 to 0.2782 min^{-1} (Fig. 3f), and it might be ascribed to the scavenging of oxidative radicals by the relatively excessive dosage of HA-FOD and H_2O_2 as discussed. However, as the MB concentration increased from 50 to 80 mg/L, the degradation rate decreased from 97.64 to 86.41%, and *k* reduced from 0.4747 to 0.1742 min^{-1}, respectively. This variation

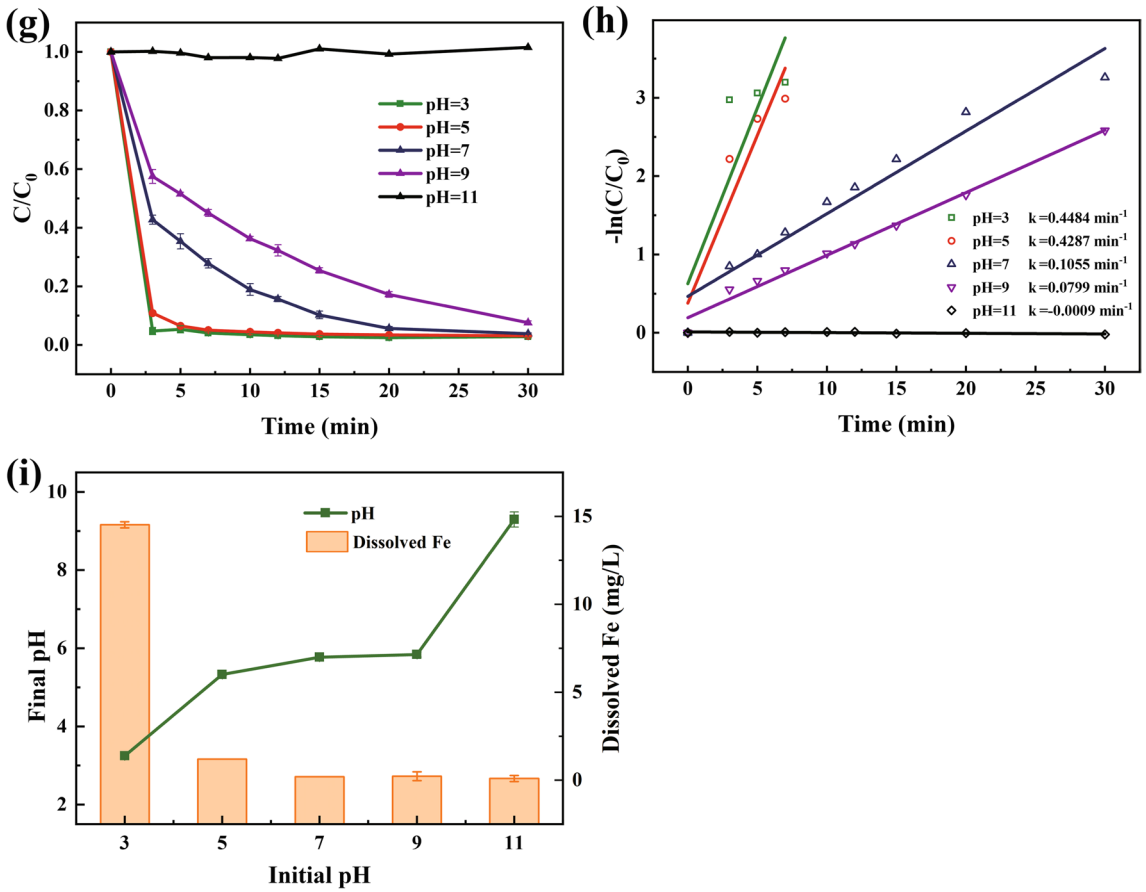

Fig. 3 (continued)

trend could be explained by that HA-FOD and H_2O_2 were relatively insufficient with MB concentration rising, and more MB molecules adsorbed on the active sites as the MB concentration rose, impeding the decomposition of H_2O_2 over the catalyst and reducing the production of •OH (Gan et al. 2018).

The Fenton process was greatly influenced by the initial pH of the solution as illustrated in Fig. 3g. HA-FOD has a wide operational pH value range of 3.0, 5.0, 7.0, and 9.0 with the corresponding product degradation ratio of 97.15, 96.88, 96.16, and 92.42%. In fact, MB was at a delayed degradation under alkaline conditions, which was in good agreement with the previous study (Hu et al. 2019). The catalytic rate constant is shown in Fig. 3h varied significantly from 0.4484 min^{-1} (pH = 3.0) to 0.0009 min^{-1} (pH = 11.0), which suggested that the variation of pH might have a strong impact on •OH generation. In an acidic environment, H_2O_2 was facilitated to produce •OH (Eq. (3)), but it preferentially decomposed into H_2O and O_2 rather than generating hydroxyl radicals, which could hinder the Fenton degradation process (Eqs. (4)–(5)) (Zhu et al. 2020; Nie et al. 2022).

$$Fe^{2+} + H_2O_2 \rightarrow Fe^{3+} + \bullet OH + OH^- \quad (3)$$

$$OH^- + H_2O_2 \rightarrow \bullet HO_2^- + H_2O \quad (4)$$

$$\bullet HO_2^- + H_2O_2 \rightarrow O_2 + H_2O + OH^- \quad (5)$$

The redox potential of •OH is + 2.8 V in the acidic solution, higher than that of + 1.5 V in the basic solution with stronger oxidation properties (Liu et al. 2022). However, reaction rate increased inconspicuously as pH declined from 5.0 to 3.0, which might be ascribed to that superfluous H^+ could consume •OH and Fe^{2+} as shown in Eq. (6).

$$\bullet OH + H^+ + Fe^{2+} \rightarrow H_2O + Fe^{3+} \quad (6)$$

The variations of solution pH values before and after the reaction are shown in Fig. 3i. The catalyst dissolved and more iron leached into the solution at lower pH, participating in the homogeneous Fenton reaction and speeding up the reaction. However, it resulted in the reduction of catalytic performance and loss of iron species and may participate as iron sludge that would cause a secondary pollution to the

environment (Zhang et al. 2019). It can be observed that while the starting pH ranged from 3.0 to 5.0, the pH after treatment was from 3.3 to 5.3, and the final pH range was from 5.8 to 9.3 with original pH value rising from 6.0 to 9.0. This result might be attributed to H^+ consumption during Fenton process as Eq. (5). While at a higher pH condition, FOD is deprotonated due to its pH buffering ability in the solution (Huang et al. 2022). Therefore, pH value of 5.0 was chosen as the optimal condition.

The optimized conditions for the photo-Fenton degradation of MB by HA-FOD are shown in Table 2 and were compared with other FOD catalysts in previous studies. The results showed that the efficiency of dye degradation by HA-FOD did not differ significantly from that of earlier studies, while HA-FOD photo-Fenton reaction had the lowest FOD and H_2O_2 dosage and the shortest reaction time, proving the high catalytic performance of HA-FOD on H_2O_2 activation. Moreover, HA-FOD was able to degrade higher concentration of MB under neutral pH environment, which was superior to previous FOD catalysts, indicating the high photo-Fenton catalytic capacity of HA-FOD.

Contribution of ROSs

Quenching experiments were performed to evaluate the contribution of ROSs on HA-FOD Fenton degradation of MB by adding specific scavengers to eliminate the relevant ROSs. Specifically, 0.3 mol/L of ethanol, isopropanol, and chloroform were used to track all of the ROSs, •OH, and $\bullet O_2^-$, respectively (Guo et al. 2021; Nie et al. 2022). As shown in Fig. 4a, a slight reduction of MB concentration was observed as ethanol was introduced to the Fenton system with a degradation rate of 7.44%, suggesting that ROSs played a prominent part in the HA-FOD Fenton system. Isopropanol could significantly slow down the breakdown of MB as its eventual degradation rate at 10.71%. This phenomenon indicated that MB degradation was predominantly ascribed to the •OH radicals. Chloroform also slowed down the degradation of MB, with a 55.26% drop of MB concentration. Although $\bullet O_2^-$ was a weak radical compared with •OH, it could convert to •OH, hence participating indirectly in the Fenton degradation of MB.

Cyclic stability evaluation for HA-FOD

To assess the cyclic stability of HA-FOD in photo-Fenton degradation of MB, successive experiments were performed as shown in Fig. 4b. The degradation rate reduced gradually during the three consecutive runs with the optimal reaction parameters of HA-FOD 0.1 g/L, H_2O_2 20 mg/L, MB 50 mg/L, and pH 5.0. Whereas on the third cycle, the degradation efficiency could still reach 82.04% as the reaction time was increased to 45 min. This declined reaction rate might be partly attributed to the deterioration of active sites on the catalyst surface with a small amount of iron leached into the solution. In addition, considering the tiny dosage of HA-FOD in this research, the aggregation and the loss of Fenton catalysts during the washing and recycling process also have a partial effect on the reduction of catalytic performance. Considering the low cost of HA-FOD recycled from solid waste RM (Ma et al. 2020), the cyclic efficiency could be improved by adding the dosage of the catalyst.

MB removal mechanism analysis

To investigate the mechanism of HA-FOD on Fenton degradation of MB, the catalysts after successive reaction were characterized by SEM (Fig. 4c), FTIR (Fig. 4d), and XPS (Fig. 4e–f). The etch of HA-FOD microstructure after Fenton reaction was observed in the SEM image, while most of the HA-FOD particles maintained regular cuboid-like microrod structure, indicating its stable catalytic ability. The EDS spectrum in Fig. 4c showed the appearance of N and S signal with the content of 3.0% and 7.7%, respectively, which inferred the adherence of MB on the surface of HA-FOD.

In comparison with the original HA-FOD, the FTIR characteristic peaks of the recycled HA-FOD were obviously reduced to a certain extent, and the peak shape gradually approached that of MB (Fig. 4d). The vibrations of the aromatic hydrocarbon ring skeleton characteristic peaks were found at 1598, 1490, and 873 cm^{-1}, and the peaks of C-N stretching vibration were observed at 1384 cm^{-1} and 1354 cm^{-1}. The peak at 1440 cm^{-1} and 1176 cm^{-1} were assigned to CH_3 group and N = Q = N stretching vibration, respectively (Wang et al. 2019b). The results indicated that

Table 2 The comparison of photo-Fenton catalytic capacity on dyes with different catalysts

Catalyst	Optimal conditions	Degradation efficiency	Reaction time	Reference
α-FOD photocatalysis	FOD 1 g/L, rhodamine B 10 mg/L, natural pH	96.48%	50 min	Fan et al. (2016)
α-FOD Fenton	H_2O_2 333 mg/L, FOD 0.1 g/L, rhodamine B 200 mg/L, pH 3.0	99.68%	10 min	Wang et al. (2019a)
β-FOD Fenton	H_2O_2 30 mg/L, FOD 0.5 g/L, MB 10 mg/L, pH 7.0	98.4%	10 min	Hu et al. (2019)
β-FOD Fenton	H_2O_2 23 mg/L, FOD 0.5 g/L, MB 20 mg/L, pH 5.5 ± 0.5	98%	3 h	Kim et al. (2020)
β-FOD Fenton	H_2O_2 20 mg/L, HA-FOD 0.1 g/L, MB 50 mg/L, pH 5.0	97.64%	10 min	This study

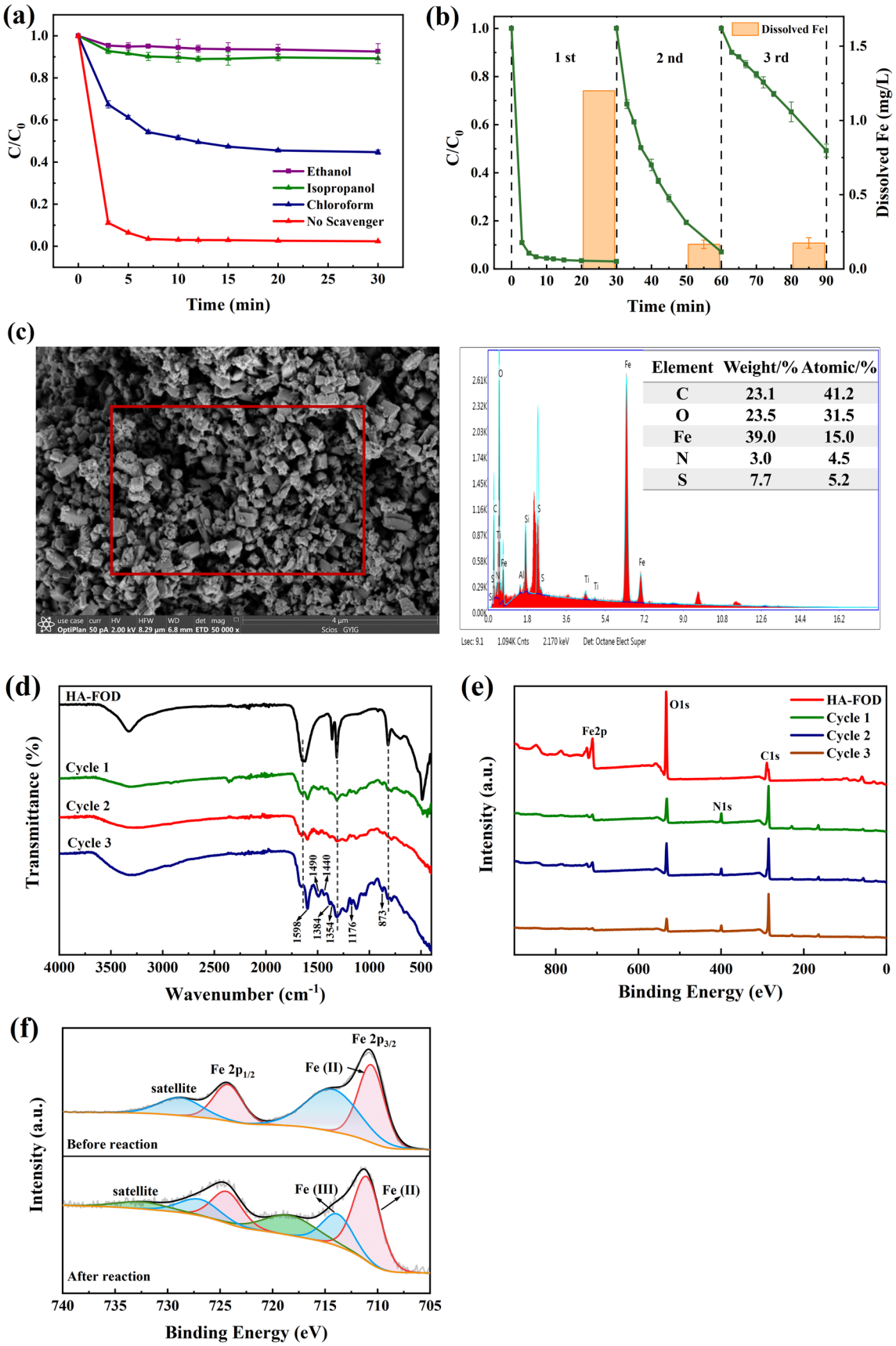
(a)
C/C0
Time (min)
Ethanol
Isopropanol
Chloroform
No Scavenger
(b)
1 st
2 nd
3 rd
Dissolved Fe
C/C0
Dissolved Fe (mg/L)
Time (min)
(c)
Element Weight/% Atomic/%
C 23.1 41.2
O 23.5 31.5
Fe 39.0 15.0
N 3.0 4.5
S 7.7 5.2
(d)
HA-FOD
Cycle 1
Cycle 2
Cycle 3
1598
1490
1440
1384
1354
1176
873
Transmittance (%)
Wavenumber (cm-1)
(e)
HA-FOD
Cycle 1
Cycle 2
Cycle 3
O1s
Fe2p
C1s
N1s
Intensity (a.u.)
Binding Energy (eV)
(f)
Fe 2p3/2
Fe 2p1/2
Fe (II)
satellite
Before reaction
satellite
Fe (III)
Fe (II)
After reaction
Intensity (a.u.)
Binding Energy (eV)

◂**Fig. 4** **a** Effect of radical scavengers on the degradation of MB catalyzed by HA-FOD, **b** reusability of HA-FOD Fenton catalyst on MB removal, **c** SEM–EDS analysis of HA-FOD catalyst after MB degradation, **d** FTIR spectra of fresh and reused HA-FOD catalysts, **e** XPS spectral analysis of fresh and reused HA-FOD catalysts, and **f** XPS peak fitting curves of Fe 2p spectra

MB was adsorbed on the surface of HA-FOD, and the binding site attributed to the N atom. With regard to these results, the adsorption of MB could compete for the surficial active sites with H_2O_2, thus inhibiting the decomposition of H_2O_2 and reducing the degradation rate on MB (He et al. 2016).

The results of full XPS scan of HA-FOD (Fig. 4e) showed that C 1 s, O 1 s, and Fe 2p peaks were identified in the survey scan spectra at about 284.8, 533.1, and 712.1 eV, respectively (Wu et al. 2022). The characteristic peak of N 1 s belonging to MB was observed at 401.1 eV. Meanwhile, the intensity of C 1 s peak was significantly increased, and the relative contents of Fe and O elements decreased in the XPS spectra of the recycled HA-FOD catalysts. These results further confirmed the adsorption of MB on the interfacial active sites of HA-FOD. For the Fe 2p spectrum (Fig. 4f), the main peaks of Fe^{2+} were located at 710.68 eV and 724.28 eV, while the satellite peak was at 714.58 eV. After reactions, the peaks of Fe^{3+} were observed at the values of 713.81 eV and 726.95 eV, and the satellite peaks were at 718.35 eV and 732.41 eV (Yoo et al. 2017; Huang et al. 2022). The results proved the transformation of Fe^{2+} to Fe^{3+} during the Fenton degradation process, which could explain the decline of MB degradation efficiency after consecutive experiments.

Conclusions

In summary, hydroxylamine hydrochloride was employed to reduce Fe^{3+} in soluble ferrioxalate complex solution leached from RM and could keep the system in a lower pH value via a hydrothermal process. HA-FOD was synthesized with a submicron size ranging from 100 nm to 1 μm with less impurity contents. This catalyst could effectively remove MB with improved photo-Fenton catalytic and photocatalytic capacities in comparison with the other two FOD catalysts obtained under UV or natural light irradiation. The combined photocatalysis and photo-Fenton method could save more than 20% of the H_2O_2, lowering reagent cost in practical sewage treatment process. The optimal experimental variables of HA-FOD in photo-Fenton process on the degradation of MB were as follows: catalyst dosage HA-FOD 0.1 g/L, H_2O_2 20 mg/L, MB 50 mg/L, and pH 5.0, and under the conditions, the final degradation efficiency of 97.64% on MB was obtained in 10 min. Scavenger experiments suggested that •OH was the major ROSs accountable for MB degradation. Furthermore, the catalyst was cyclic stable after two repeated experiments, and the adsorption of MB on the surface of HA-FOD competed for the active sites with H_2O_2, thus contributing to the further declined reusability of the catalyst. This study provides a new method to synthesize ferrous oxalate from red mud with high Fenton catalytic performance and also provides a perspective on utilizing iron-rich industrial waste to prepare HA-FOD mineral clusters to remediate organically polluted wastewater through the novel synthetic method.

Supplementary information The online version contains supplementary material available at https://doi.org/10.1007/s11356-023-28308-z.

Acknowledgements All authors wish to thank Prof. Wan's Group for FTIR determination.

Author contribution Yuxin Yang: Investigation, resources, data curation, writing—original draft. Ning Wang: Conceptualization, resources, supervision. Hannian Gu: Writing—review and editing, conceptualization, validation, resources, methodology, supervision, funding acquisition.

Funding The current research was funded by the National Natural Science Foundation of China (U1812402), the Youth Innovation Promotion Association, CAS (2021400), and Guizhou Outstanding Young Scientific and Technological Talents Project (2021–5641).

Data availability The authors confirm that the data supporting the findings of this study are available within the article and its supplementary materials.

Declarations

Ethics approval and consent to participate Not applicable.

Consent for publication The authors are willing to permit the Journal to publish the article.

Competing interests The authors declare no competing interests.

References

Agrawal S, Dhawan N (2021) Evaluation of red mud as a polymetallic source - a review. Miner Eng 171:107084. https://doi.org/10.1016/j.mineng.2021.107084

Angermann A, Töpfer J (2008) Synthesis of magnetite nanoparticles by thermal decomposition of ferrous oxalate dihydrate. J Mater Sci 43:5123–5130. https://doi.org/10.1007/s10853-008-2738-3

Baba Y, Yatagai T, Harada T, Kawase Y (2015) Hydroxyl radical generation in the photo-Fenton process: effects of carboxylic acids on iron redox cycling. Chem Eng J 277:229–241. https://doi.org/10.1016/j.cej.2015.04.103

Bento NI, Santos PSC, de Souza TE, Oliveira LCA, Castro CS (2016) Composites based on PET and red mud residues as catalyst for organic removal from water. J Hazard Mater 314:304–311. https://doi.org/10.1016/j.jhazmat.2016.04.066

Bi W, Dong W (2021) The degradation of oxytetracycline with ferrous oxalate under different light irradiation. Environ Technol 42:1084–1091. https://doi.org/10.1080/09593330.2019.1652698

Brillas EF (2022) Fenton, photo-Fenton, electro-Fenton, and their combined treatments for the removal of insecticides from waters and soils A review. Sep Purif Technol 284:120290. https://doi.org/10.1016/j.seppur.2021.120290

Chen N, Zhao Y, Li M, Wang X, Peng X, Sun H, Zhang L (2022) $FeC_2O_4 \bullet 2H_2O$ enables sustainable conversion of hydrogen peroxide to hydroxyl radical for promoted mineralization and detoxification of sulfadimidine. J Hazard Mater 436:129049. https://doi.org/10.1016/j.jhazmat.2022.129049

Dhal JP, Mishra BG, Hota G (2015) Ferrous oxalate, maghemite and hematite nanorods as efficient adsorbents for decontamination of Congo red dye from aqueous system. Int J Environ Sci Technol 12:1845–1856. https://doi.org/10.1007/s13762-014-0535-x

Dias IN, Souza BS, Pereira JHOS, Moreira FC, Dezotti M, Boaventura RAR, Vilar VJP (2014) Enhancement of the photo-Fenton reaction at near neutral pH through the use of ferrioxalate complexes: a case study on trimethoprim and sulfamethoxazole antibiotics removal from aqueous solutions. Chem Eng J 247:302–313. https://doi.org/10.1016/j.cej.2014.03.020

Fan X, Zhang L, Li M, Wang M, Zhou X, Cheng R, Zhou Y, Shi J (2016) α-Ferrous oxalate dihydrate: a simple coordination polymer featuring photocatalytic and photo-initiated Fenton oxidations. Sci China Mater 59:574–580. https://doi.org/10.1007/s40843-016-5064-y

Ferroudj N, Talbot D, Michel A, Davidson A, Abramson S (2017) Increasing the efficiency of magnetic heterogeneous Fenton catalysts with a simple halogen visible lamp. J Photochem Photobiol A 338:85–95. https://doi.org/10.1016/j.jphotochem.2017.01.029

Gan L, Li B, Guo M, Weng X, Wang T, Chen Z (2018) Mechanism for removing 2,4-dichlorophenol via adsorption and Fenton-like oxidation using iron-based nanoparticles. Chemosphere 206:168–174. https://doi.org/10.1016/j.chemosphere.2018.04.162

Gu H, Hargreaves JSJ, Jiang J-Q, Rico JL (2017) Potential routes to obtain value-added iron-containing compounds from red mud. J Sustain Metall 3:561–569. https://doi.org/10.1007/s40831-016-0112-2

Guo X, Jia J, Xu Y, Meng Q, Zha F, Tang X, Tian H (2021) FeS_2-$Fe_{1-x}S$ heterostructure as a high-efficient Fenton-like catalyst for ultrafast degradation of orange II. Appl Surf Sci 556:149786. https://doi.org/10.1016/j.apsusc.2021.149786

Hajjaji W, Pullar RC, Labrincha JA, Rocha F (2016) Aqueous Acid Orange 7 dye removal by clay and red mud mixes. Appl Clay Sci 126:197–206. https://doi.org/10.1016/j.clay.2016.03.016

He J, Yang X, Men B, Wang D (2016) Interfacial mechanisms of heterogenous Fenton reactions catalyzed by iron-based materials: a review. J Environ Sci 39:97–109. https://doi.org/10.1016/j.jes.2015.12.003

Hu L, Wang P, Xiong S, Chen S, Yin X, Wang L, Wang H (2019) The attractive efficiency contributed by the in-situ reactivation of ferrous oxalate in heterogeneous Fenton process. Appl Surf Sci 467–468:185–192. https://doi.org/10.1016/j.apsusc.2018.10.151

Huang Q, Cai X, Chen M, Yang Q, Fan S, Zhang Y, Hu H, Gan T, Huang Z (2022) A stepwise processing strategy for treating manganese residue and the remediation of hexavalent chromium in water and soil by manganese residue-derived (Fe, Mn)C2O4. Chem Eng J 436:135258. https://doi.org/10.1016/j.cej.2022.135258

Karimi S, Shokri A, Aghel B (2020) Remediation of spent caustic in the wastewater of oil refinery by photo-Fenton process. Arch Hyg Sci 9:179–188. https://doi.org/10.29252/archhygsci.9.3.179

Khairul MA, Zanganeh J, Moghtaderi B (2019) The composition, recycling and utilisation of Bayer red mud. Resour Conserv Recycl 141:483–498. https://doi.org/10.1016/j.resconrec.2018.11.006

Kim EJ, Baek K (2019) Selective recovery of ferrous oxalate and removal of arsenic and other metals from soil-washing wastewater using a reduction reaction. J Clean Prod 221:635–643. https://doi.org/10.1016/j.jclepro.2019.03.014

Kim SR, Kim S, Kim EJ (2020) Photoreaction characteristics of ferrous oxalate recovered from wastewater. Chemosphere 249:126201. https://doi.org/10.1016/j.chemosphere.2020.126201

Lai C, Shi X, Li L, Cheng M, Liu X, Liu S, Li B, Yi H, Qin L, Zhang M, An N (2021) Enhancing iron redox cycling for promoting heterogeneous Fenton performance: a review. Sci Total Environ 775:145850. https://doi.org/10.1016/j.scitotenv.2021.145850

Li K, Liang Y, Yang J, Yang G, Xu R, Xie X (2018) α-Ferrous oxalate dihydrate: an Fe-based one-dimensional metal organic framework with extraordinary photocatalytic and Fenton activities. Catal Sci Technol 8:6057–6061. https://doi.org/10.1039/c8cy01779d

Li H, Chai W, Cao Y, Yang S (2022a) Flotation enhancement of low-grade bauxite using oxalic acid as surface pretreatment agent. Appl Surf Sci 577:151964. https://doi.org/10.1016/j.apsusc.2021.151964

Li W, Li Z, Wang N, Gu H (2022b) Selective extraction of rare earth elements from red mud using oxalic and sulfuric acids. J Environ Chem Eng 10:108650. https://doi.org/10.1016/j.jece.2022.108650

Li Z, Gu H, Hong B, Wang N, Chen M (2022c) An innovative process for dealkalization of red mud using leachate from Mn-containing waste. J Environ Chem Eng 10:107222. https://doi.org/10.1016/j.jece.2022.107222

Lin R, Li Y, Yong T, Cao W, Wu J, Shen Y (2022) Synergistic effects of oxidation, coagulation and adsorption in the integrated Fenton-based process for wastewater treatment: a review. J Environ Manage 306:114460. https://doi.org/10.1016/j.jenvman.2022.114460

Liu Z-J, Liu W, Wang Y, Guo M-L (2016) Preparation of β-ferrous oxalate dihydrate layered nanosheets by mechanochemical method and its visible-light-driven photocatalytic performance. Mater Lett 178:83–86. https://doi.org/10.1016/j.matlet.2016.04.201

Liu S, Yu B, Wang S, Shen Y, Cong H (2020) Preparation, surface functionalization and application of Fe_3O_4 magnetic nanoparticles. Adv Colloid Interface Sci 281:102165. https://doi.org/10.1016/j.cis.2020.102165

Liu X, Han Y, He F, Gao P, Yuan S (2021) Characteristic, hazard and iron recovery technology of red mud - a critical review. J Hazard Mater 420:126542. https://doi.org/10.1016/j.jhazmat.2021.126542

Liu Y, Wang X, Sun Q, Yuan M, Sun Z, Xia S, Zhao J (2022) Enhanced visible light photo-Fenton-like degradation of tetracyclines by expanded perlite supported $FeMo_3O_x$/g-C_3N_4 floating Z-scheme catalyst. J Hazard Mater 424:127387. https://doi.org/10.1016/j.jhazmat.2021.127387

Ma S, Gu H, Mei Z, Yang Y, Wang N (2020) Conversion synthesis of manganese sulfate residue into iron hydroxide adsorbent for Cu(II) removal from aqueous solution. Environ Sci Pollut Res 27:23871–23879. https://doi.org/10.1007/s11356-020-08819-9

Miklos DB, Remy C, Jekel M, Linden KG, Drewes JE, Hübner U (2018) Evaluation of advanced oxidation processes for water and wastewater treatment - a critical review. Water Res 139:118–131. https://doi.org/10.1016/j.watres.2018.03.042

Mohadesi M, Aghel B, Razmegir MH (2021) COD reduction in petrochemical wastewater using the solar photo-Fenton process. J Chem Petro Eng 55:69–81. https://doi.org/10.22059/jchpe.2020.310442.1330

Mohamed HH, Besisa DHA (2022) Eco-friendly and solar light-active Ti-Fe_2O_3 ellipsoidal capsules' nanostructure for removal of herbicides and organic dyes. Environ Sci Pollut Res 2022:1–11. https://doi.org/10.1007/s11356-022-23119-0

Nie X, Li G, Li S, Luo Y, Luo W, Wan Q, An T (2022) Highly efficient adsorption and catalytic degradation of ciprofloxacin by a novel heterogeneous Fenton catalyst of hexapod-like pyrite nanosheets

mineral clusters. Appl Catal B 300:120734. https://doi.org/10.1016/j.apcatb.2021.120734
Niveditha SV, Gandhimathi R (2020) Flyash augmented Fe_3O_4 as a heterogeneous catalyst for degradation of stabilized landfill leachate in Fenton process. Chemosphere 242:125189. https://doi.org/10.1016/j.chemosphere.2019.125189
Oturan MA, Aaron J-J (2014) Advanced oxidation processes in water/wastewater treatment: principles and applications. A review. Crit Rev Environ Sci Technol 44:2577–2641. https://doi.org/10.1080/10643389.2013.829765
Peng S, Zhang W, He J, Yang X, Wang D, Zeng G (2016) Enhancement of Fenton oxidation for removing organic matter from hypersaline solution by accelerating ferric system with hydroxylamine hydrochloride and benzoquinone. J Environ Sci 41:16–23. https://doi.org/10.1016/j.jes.2015.05.006
Pliego G, Zazo JA, Garcia-Muñoz P, Munoz M, Casas JA, Rodriguez JJ (2015) Trends in the intensification of the Fenton process for wastewater treatment: an overview. Crit Rev Environ Sci Technol 45:2611–2692. https://doi.org/10.1080/10643389.2015.1025646
Rahimi M, Aghel B, Sadeghi M, Ahmadi M (2014) Using Y-shaped microreactor for continuous decolorization of an Azo dye. Desalin Water Treat 52:5513–5519. https://doi.org/10.1080/19443994.2013.807471
Ribeiro JP, Nunes MI (2021) Recent trends and developments in Fenton processes for industrial wastewater treatment - a critical review. Environ Res 197:110957–110973. https://doi.org/10.1016/j.envres.2021.110957
Samal S (2021) Utilization of red mud as a source for metal ions - a review. Materials (basel) 14:2211. https://doi.org/10.3390/ma14092211
Samsami S, Mohamadizaniani M, Sarrafzadeh M-H, Rene ER, Firoozbahr M (2020) Recent advances in the treatment of dye-containing wastewater from textile industries: overview and perspectives. Process Saf Environ Prot 143:138–163. https://doi.org/10.1016/j.psep.2020.05.034
Sukhatskiy Y, Sozanskyi M, Shepida M, Znak Z, Gogate PR (2022) Decolorization of an aqueous solution of methylene blue using a combination of ultrasound and peroxate process. Sep Purif Technol 288:120651. https://doi.org/10.1016/j.seppur.2022.120651
Tanvar H, Mishra B (2021) Hydrometallurgical recycling of red mud to produce materials for industrial applications: alkali separation, iron leaching and extraction. Metall Mater Trans B 52:3543–3557. https://doi.org/10.1007/s11663-021-02285-5
Tkaczyk A, Mitrowska K, Posyniak A (2020) Synthetic organic dyes as contaminants of the aquatic environment and their implications for ecosystems: a review. Sci Total Environ 717:137222. https://doi.org/10.1016/j.scitotenv.2020.137222
Vorontsov AV (2019) Advancing Fenton and photo-Fenton water treatment through the catalyst design. J Hazard Mater 372:103–112. https://doi.org/10.1016/j.jhazmat.2018.04.033
Wang J, Tang J (2021) Fe-based Fenton-like catalysts for water treatment: preparation, characterization and modification. Chemosphere 276:130177. https://doi.org/10.1016/j.chemosphere.2021.130177
Wang F, Wu Y, Gao Y, Li H, Chen Z (2016) Effect of humic acid, oxalate and phosphate on Fenton-like oxidation of microcystin-LR by nanoscale zero-valent iron. Sep Purif Technol 170:337–343. https://doi.org/10.1016/j.seppur.2016.06.046
Wang G, Zhou A, Xu Q (2019a) α-Ferrous oxalate with different micro scale: synthesis and catalytic degradation effect to rhodamine B. Solid State Sci 91:54–60. https://doi.org/10.1016/j.solidstatesciences.2019.03.004
Wang N, Chen J, Wang J, Feng J, Yan W (2019b) Removal of methylene blue by polyaniline/TiO_2 hydrate: adsorption kinetic, isotherm and mechanism studies. Powder Technol 347:93–102. https://doi.org/10.1016/j.powtec.2019.02.049
Wang Z, Qiu W, Pang S, Jiang J (2019c) Effect of chelators on the production and nature of the reactive intermediates formed in Fe(II) activated peroxydisulfate and hydrogen peroxide processes. Water Res 164:114957. https://doi.org/10.1016/j.watres.2019.114957
Wang J, Kang D, Shen B, Sun H (2020) Wu C (2020) Enhanced hydrogen production from catalytic biomass gasification with in-situ CO_2 capture. Environ Pollut 267:115487. https://doi.org/10.1016/j.envpol.2020.115487
Wu S, Deng S, Ma Z, Liu Y, Yang Y, Jiang Y (2022) Ferrous oxalate covered ZVI through ball-milling for enhanced catalytic oxidation of organic contaminants with persulfate. Chemosphere 287:132421. https://doi.org/10.1016/j.chemosphere.2021.132421
Xue S, Wu Y, Li Y, Kong X, Zhu F, Hartley W, Li X, Ye Y (2019) Industrial wastes applications for alkalinity regulation in bauxite residue: a comprehensive review. J Cent South Univ 26:268–288. https://doi.org/10.1007/s11771-019-4000-3
Yoo SH, Jang D, Joh H-I, Lee S (2017) Iron oxide/porous carbon as a heterogeneous Fenton catalyst for fast decomposition of hydrogen peroxide and efficient removal of methylene blue. J Mater Chem A 5:748–755. https://doi.org/10.1039/C6TA07457J
Yu Z-L, Shi Z-X, Chen Y-M, Niu Y-J, Wang Y-X, Wan P-Y (2012) Red-mud treatment using oxalic acid by UV irradiation assistance. Trans Nonferr Metal Soc China 22:456–460. https://doi.org/10.1016/S1003-6326(11)61198-9
Zeng Q, Huang Y, Huang L, Hu L, Xiong D, Zhong H, He Z (2020) Efficient removal of hexavalent chromium in a wide pH range by composite of SiO_2 supported nano ferrous oxalate. Chem Eng J 383:123209. https://doi.org/10.1016/j.cej.2019.123209
Zeng Q, Wang S, Hu L, Zhong H, He Z, Sun W, Xiong D (2021) Oxalic acid modified copper tailings as an efficient adsorbent with super high capacities for the removal of Pb2+. Chemosphere 263:127833. https://doi.org/10.1016/j.chemosphere.2020.127833
Zhang Y, Zhou M (2019) A critical review of the application of chelating agents to enable Fenton and Fenton-like reactions at high pH values. J Hazard Mater 362:436–450. https://doi.org/10.1016/j.jhazmat.2018.09.035
Zhang M, Dong H, Zhao L, Wang D, Meng D (2019) A review on Fenton process for organic wastewater treatment based on optimization perspective. Sci Total Environ 670:110–121. https://doi.org/10.1016/j.scitotenv.2019.03.180
Zhu X, Li J, Xie B, Feng D, Li Y (2020) Accelerating effects of biochar for pyrite-catalyzed Fenton-like oxidation of herbicide 2,4-D. Chem Eng J 391:123605. https://doi.org/10.1016/j.cej.2019.123605